Optical studies of the smectic-C^*_α phase layer structure in free-standing films

D. A. Olson,[1] S. Pankratz,[1,*] P. M. Johnson,[1,†] A. Cady,[1] H. T. Nguyen,[2] and C. C. Huang[1]

[1]*School of Physics and Astronomy, University of Minnesota, Minneapolis, Minnesota 55455*

[2]*Centre de Recherche Paul Pascal, CNRS, Université Bordeaux I, Avenue A. Schweitzer, F-33600 Pessac, France*

(Received 15 November 2000; published 24 May 2001)

The layer structure of the smectic-C^*_α phase of one liquid-crystal compound has been acquired from both differential optical reflectivity and ellipsometry measurements in the free-standing film geometry. The data from both techniques display characteristic oscillations as a function of temperature, which can be described by a model for the film consisting of surface anticlinic layers and an interior short-pitched azimuthal helix. These results are consistent with those found previously for another compound. Depolarized reflected light microscopy is used to study the films when the unique features of the aforementioned oscillations occur.

DOI: 10.1103/PhysRevE.63.061711 PACS number(s): 61.30.Gd, 77.84.Nh

I. INTRODUCTION

Soon after the discovery of the smectic-C^*_A phase in one liquid-crystal compound [1], three intermediate smectic-C^* variant phases, namely, smectic-C^*_α, smectic-C^*_{FI2}, and smectic-C^*_{FI1}, were identified [2]. Upon cooling the complete transition sequence below smectic-A is smectic-C^*_α - smectic-C^* - smectic-C^*_{FI2} - smectic-C^*_{FI1} - smectic-C^*_A, where the * signifies a chiral phase. Similar to the smectic-A phase, all five of these smectic-C phases exhibit liquidlike positional order within each smectic layer but the molecules in each layer possess an average tilt (θ) with respect to the layer normal. From previous x-ray scattering experiments, it is known that the bulk tilt angle (θ_b) is spatially homogeneous in all five tilted phases [3,4] and is a function of temperature. These tilted phases are distinguished by the azimuthal arrangements of their layers. Numerous experimental efforts have been made to obtain the molecular orientational arrangements in three intermediate smectic-C^* variant phases [2,5]. The most direct structural information has been acquired by resonant x-ray scattering from free-standing films of several specially prepared liquid-crystal compounds [4,6,7], e.g., 10OTBBB1M7 [see Fig. 1(a)]. Subsequent high-resolution optical reflectivity and null-transmission ellipsometry investigations have allowed us to determine the molecular azimuthal orientations in these three intermediate smectic-C^* variant phases [8,9]. Our experimental results obtained from the smectic-C^*_α phase of 10OTBBB1M7, differ in their details from those of another liquid-crystal compound reported by Schlauf *et al.* [10]. Consequently, detailed studies of another compound are essential. In this paper we present optical results for [4-(1-methylheptoloxcarbonyl)phenyl4′-octylbiphenyl-4-carboxylate] (MHPBC) in the smectic-C^*_α phase. The chemical structure of MHPBC is given in Fig. 1(b).

While resonant x rays are very powerful at determining the layer structure they have the shortcoming that only specially prepared compounds can be used, i.e., those containing a sulfur or selenium atom in their core. They also need to be performed at high-intensity x-ray sources. For these reasons it is necessary to develop other techniques for studying these phases. To this end we have developed two optical systems: high-resolution differential reflectivity [11] and null-transmission ellipsometry [12]. These techniques have unveiled information about both the interior and surface structures of free-standing films [8,9,13].

The first use of our high-resolution optical systems was to take reflectivity and ellipsometry data from free-standing films of 10OTBBB1M7 of various thicknesses [8]. By using this compound we could compare the optical results to the resonant x-rays results. We found that upon cooling through the smectic-C^*_α phase range, the data from ellipsometry and the reflectivity of linearly polarized light display characteristic reproducible oscillations as a function of temperature. Six observations regarding these oscillations have been made. First, each oscillation displays a reproducible discontinuous jump. Second, the oscillation frequency in temperature space (f) is roughly constant. Third, f decreases linearly with the number of smectic layers (N) of the film. The finite intercept of f versus N indicates that there are approximately 18 surface layers in the films. Fourth, the amplitude of oscillation is roughly independent of N. Fifth, the basic features show

a) 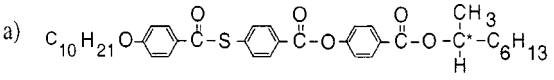

Isotropic (152.6) SmA (123.6) SmC $^*_\alpha$(120.2) SmC *(119.2)
SmC $^*_{FI2}$ (114) SmC $^*_{FI1}$ (112) SmC $^*_A$ (109.7) Crystal

b) 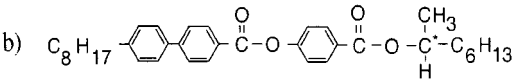

Isotropic (109) SmA (76) SmC $^*_\alpha$(72) SmC $^*_{FI2}$ (68)
SmC $^*_{FI1}$ (65) SmC $^*_A$ (60) Crystal

FIG. 1. (a) and (b) show the molecular structure and bulk phase sequence for 10OTBBB1M7 and MHPBC, respectively. The transition temperatures are in degrees centigrade.

*Present address: 3M Center, St. Paul, MN 55144.

†Present address: Van der Waals-Zeeman Institute, University of Amsterdam, Amsterdam, The Netherlands.

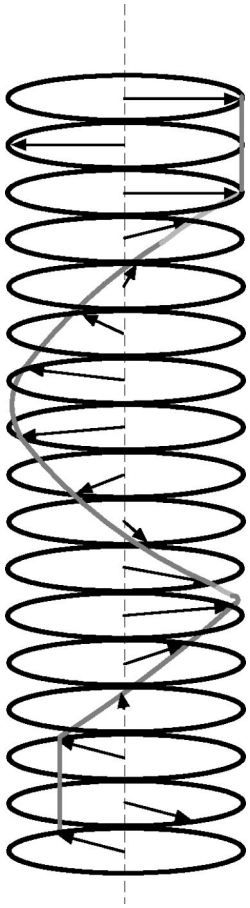

FIG. 2. A short-pitch helical structure with anticlinic tilted surface layers, shown by the projection of the molecular director in the layer plan, i.e., the *c* director for each layer.

little change under reversal of the applied electric field. Sixth, the oscillations do not occur in the reflected intensity of circularly polarized incident light.

To explain the first feature, we proposed that the layer structure of the film changes its azimuthal orientation by 180° under the constant applied electric field at certain T. This is due to the net polarization of the film passing through zero at these temperatures. The third and fourth features indicate that the frequency and amplitude of the oscillations are properties of interior and surface layers, respectively. Although our optical data suffered from an inversion problem, i.e., different layer profiles may lead to the similar set of data, these unique characteristics along with the resonant x-ray diffraction data allow us to propose a model as sketched in Fig. 2. The film consists of surface anticlinic layers of a larger surface-induced tilt angle (θ_s) which exponentially decreases (with penetration length ξ) toward a smaller θ_b [14]. The interior layers have a short-pitched azimuthal helix with a pitch that changes linearly from 5 to 8 layers as the temperature increases from the low- to high-temperature end of smectic-C_α^*, as was determined from resonant x rays [6]. Such a model yields an excellent description of our optical data [8]. It is worth noting that the surface-induced optically biaxial layers that are coupled to the interior layers are what allowed us to gain significant physical insight into the optically uniaxial interior layers.

Meanwhile, Schlauf *et al.* [10], reported their ellipsometry studies of the smectic-C_α^* structure from another liquid-crystal compound (11HFBBB1M7) which shows the smectic-A–smectic-C_α^* - smectic-C^* - crystal phase sequence without displaying the ferri- or antiferroelectric phase. As shown in Fig. 1(a), 10OTBBB1M7 displays the ferri and antiferro phases. Below the smectic-C_α^* phase, the temperature ranges for the smectic-C^* phase are about 1 and 17 K for 10OTBBB1M7 and 11HFBBB1M7, respectively. The major differences from the above-mentioned results for 10OTBBB1M7 are the following two points. First, in Schlauf's study of 11HFBBB1M7, f increases as temperature decreases. Second, they also found that the split in the one of the ellipsometry parameters Δ, is significant under electric-field reversal and increases as temperature is decreased. Schlauf *et al.* [10] used a single surface layer with a large tilt angle ($\theta_s = 30°$) to model the ellipsometry data. In contrast, on the basis of our fourth and fifth features, we employed nine surface anticlinic layers per surface with $\theta_s = 12°$ and penetration length $\xi = 5$ layers to describe the 10OTBBB1M7 data. Finally, Schlauf *et al.* reported a nonlinear temperature variation of the short-helical pitch because f decreases as the temperature decreases.

In light of these significant differences and the fact that 10OTBBB1M7 is especially prepared for the resonant x-ray scattering studies, it became very important to acquire the smectic-C_α^* structure from another ''common'' liquid-crystal compound. One of the natural choices is MHPBC because it has a sufficiently large smectic-C_α^* temperature window for easy study [$\sim 4°$, see phase sequence in Fig. 1(b)]. This compound shows the various ferri- and antiferroelectric phases, unlike 11HFBBB1M7. MHPBC does not have a heavy atom in its core, so it cannot be studied by resonant x-ray scattering. To study this compound we have performed null-transmission ellipsometry and high-resolution differential reflectivity. To understand the discontinuous changes in the optical parameters we have also studied MHPBC using depolarized reflected light microscopy.

II. EXPERIMENTAL METHODS AND RESULTS

In our experiments, the liquid-crystal free-standing films were prepared in temperature regulated two-stage ovens [15] (temperature stability is approximately 10 mK). Two different ovens have been employed for this research project. To minimize sample degradation, the ovens were filled with He or Ar as the exchange gas. The ovens have optical accesses for our experimental probes. To obtain temperature variation of physical parameters, the typical ramp rates used were between 50 and 100 mK/min.

To analyze the results that are presented below, we used the 4×4 matrix method [16]. This method is a matrix formulation of Maxwell's equations that makes the following assumptions about the sample: the optical properties of the sample are a function of only one direction, the incident light is a plane wave, and only linear optical effects are considered. We add the following assumptions to approximately describe our free-standing films: the sample can be divided

into slabs corresponding to smectic layers where within each slab the optical properties are constant, and the magnetic permeability is 1. This method is advantageous because it rewrites Maxwell's equations for the electric- and magnetic-field vectors as four coupled first-order differential equations that can be formulated as a 4×4 transfer matrix. The propagation of the electromagnetic wave through the sample can be calculated by the transfer matrix.

In our experiments we apply an electric field in the plane of the film to align the domains. A field of 2–3 V/cm is typically used, as this aligns the sample without inducing flow or distorting the zero-field structure. Based upon smectic-C^* we assume that the polarization due to each layer is perpendicular to the tilt plane. For our simulations, we assume that the orientation of the net polarization of the film is along the sum of these individual layer polarizations. Because of the finite size of our samples, the net polarization of the film is zero only at certain values of the pitch.

A. Null-transmission ellipsometry

Null-transmission ellipsometry is an experimental procedure to measure the optical parameters of a system at a single laser wavelength ($\lambda=6328$ Å in our setup). Two optical parameters are measured: Δ and Ψ. Δ is the necessary phase lag between the *p*- and *s*- components of the incident laser beam to create linearly polarized transmitted light with polarization angle Ψ. The light passes through the sample at 45° to the normal of the film. The ellipticity of the incoming light is controlled by passing circularly polarized light through a rotatable polarizer and then a fixed quarter-wave plate. The light passes through the sample, and, if the light has the correct input ellipticity, the light emerges linearly polarized. A second rotatable polarizer is rotated to find the minimum light intensity, which measures the polarization of the output light. The angle of the first and second polarizers is measured and the angle of the quarter-wave plate is known. With this knowledge, Ψ and Δ are readily calculated using equations reported elsewhere [17,18]. Our experimental setup will be described in detail elsewhere [12].

For MHPBC $n_o=1.482\pm0.002$, $n_e=1.64\pm0.01$, and the smectic layer spacing (d) of 35.4 ± 0.2 Å was measured in the high-temperature range of the smectic-*A* phase [12]. Here n_e denotes the index of refraction along the long axis of the molecule and n_o is the index of refraction perpendicular to the long axis of the molecule. These are determined by pulling a series of films and fitting the Ψ versus Δ data. Specifically, first n_o and n_e are found by matching the height and width the loops seen in Fig. 3. d affects only the spacing between the data points and not the overall size of the loops, so it can be fit after n_o and n_e in order to get the correct spacing between data points. The value of n_e has a high variance because MHPBC retained a tilt near the surface due to the surface-air interface and it was thus impossible to capture Δ and Ψ values that were exactly what would be found for a film with no surface-induced structure. The value of Δ varies more than Ψ because Δ is more sensitive to the orientation of the film, making the uncertainty of n_e larger than that for n_o. We have found that n_o and n_e in the molecular

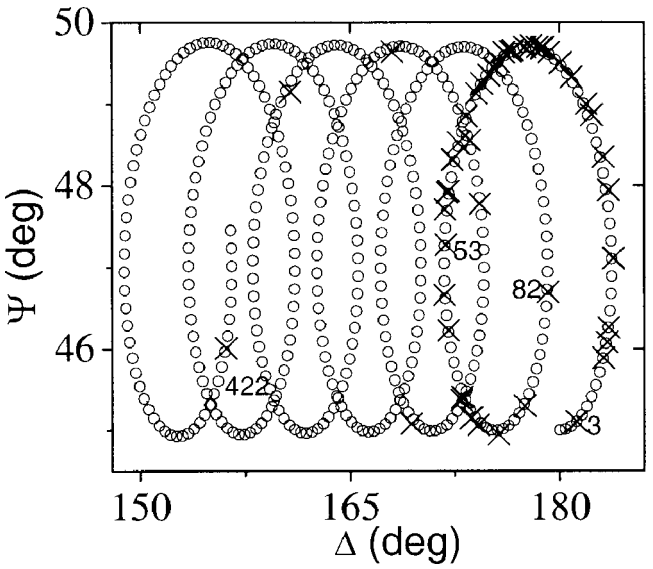

FIG. 3. Determination of n_o, n_e, and d for MHPBC. The data (crosses) were obtained by spreading 51 films of thickness varying from 3 to ~422 layers. The fit is shown with open circles. The location of several thicknesses, in units of smectic layers, are marked on the plot.

frame are not strongly temperature dependant. We have checked to determine that the values obtained at high temperatures give reasonable fits to data taken at lower temperatures.

The ellipsometry parameters (Δ and Ψ) obtained from a 65-layer MHPBC film are plotted as a function of temperature in Fig. 4. This figure shows data from two experimental

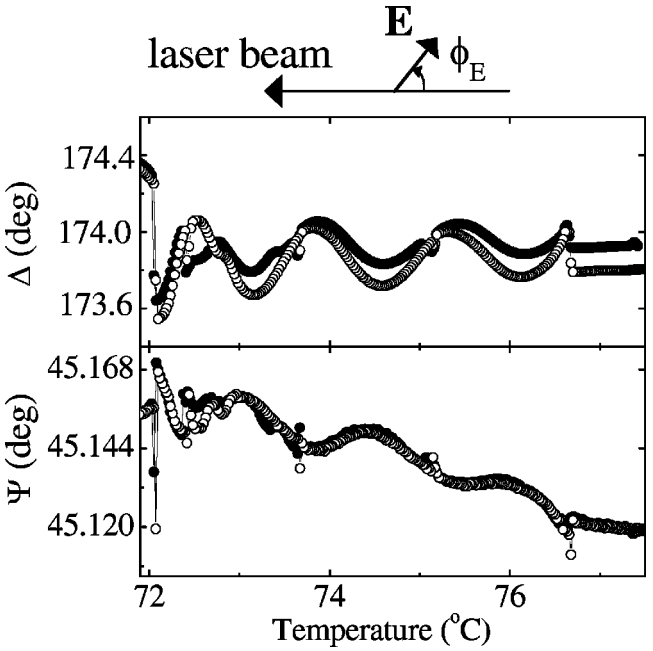

FIG. 4. Δ and Ψ versus temperature from a 65-layer MHPBC film at $\phi_E=90°$ (open circles) and $\phi_E=270°$ (solid circles). ϕ_E is shown as the angle between the electric field and the incident plane of the laser.

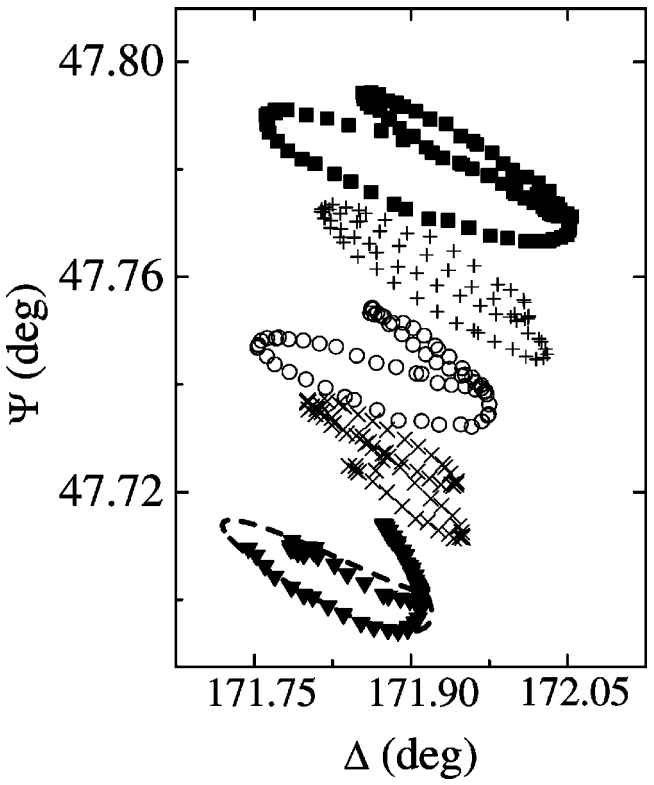

FIG. 5. Ψ versus Δ plots obtained at five different temperatures from a 53-layer MHPBC film in the smectic-*A* and smectic-C^*_α phase. The down triangles were taken in the smectic-*A* phase at a temperature of 76.8°C. The *x*'s, circles, crosses, and squares were taken in the smectic-C^*_α phase at temperatures of 76.0 °C, 75.1°C, 73.9 °C, and 73.1°C, respectively. The data taken at 73.1°C and 75.1°C are offset by 0.01° and 0.002° in Ψ, respectively, for clarity.

runs with opposite directions of applied electric field (± 2 V/cm) $\phi_E = 90°$ (open circles) and $\phi_E = 270°$ (solid circles) which are perpendicular to the optical incidence plane. ϕ_E is the angle between the electric field and the incident plane of the laser beam as shown in Fig. 4. This data confirms that the first, second, and fifth features listed above for the 10OTBBB1M7 compound, are also true for MHPBC.

To acquire additional information about the structures of the smectic-*C** variant phases, we employed a specially designed film plate made of a glass cover slide. The slide has a circular film hole (about 0.7 cm diameter) that is surrounded by eight approximately equally spaced electrodes [9]. By setting each electrode to the proper voltage, we can generate a rotatable electric field (~ 3 V/cm) in the plane of the liquid-crystal film. Typically, ϕ_E is advanced in 6° steps and it takes 1 min to acquire one reading for the ellipsometry parameters Δ and Ψ. At a given temperature, 1 h is required to complete a rotation of the electric field. Thus, we measure Δ and Ψ at 60 equally spaced azimuthal orientations for each temperature.

We conducted a detailed experimental run from a 53-layer MHPBC film using the rotatable electric field. More than 40 different Ψ and Δ plots were acquired as the film was cooled from the smectic-*A* phase. For clarity, Fig. 5 shows only five

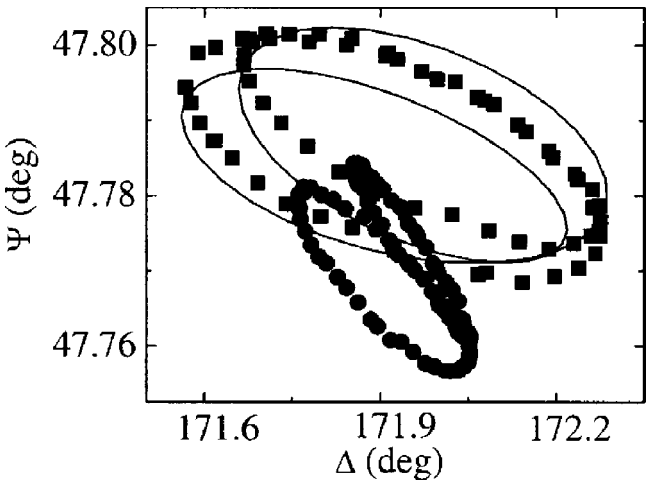

FIG. 6. Comparison of the shape of the Ψ versus Δ plots taken from a 53-layer MHPBC film in the smectic-C^*_{FI2} and smectic-C^*_α phases. The plot with circles was taken at 73.1°C in the smectic-C^*_α phase. The squares are the data taken from 71.7 °C in the smectic-C^*_{FI2} phase. A simulation of the smectic-C^*_{FI2} data is shown with a solid line.

such plots and Fig. 6 shows two. These figures respectively display characteristic changes of the Ψ versus Δ plots in both the smectic-*A*-smectic-C^*_α and smectic-C^*_α-smectic-C^*_{FI2} phase transitions.

In Fig. 5, the data obtained above the bulk smectic-*A*-smectic-C^*_α transition shown with down triangles indicates that the two sets of surface-induced layers are almost planar. A simulation (line) was made with three anticlinic layers per surface, $\theta_s = 10°$ and $\xi = 3$ layers. In particular, the shape suggests that the net tilt of the top and bottom surface layers are nearly aligned [13].

In the smectic-C^*_α phase, the interior layers have a temperature varying short helical pitch structure. In general, the two sets of surface-induced layers will not be coplanar. The size of the Ψ versus Δ plot increases gradually as the temperature decreases through the smectic-C^*_α temperature range. This clearly indicates an increase in biaxiality. We believe that this is due to the tilt-angle increase on the surface and interior layers. The drift in Ψ and Δ as a function of temperature is due to the smectic layer spacing decreasing as the temperature is decreased, as this causes the overall thickness to decrease. An interesting detail about the smectic-C^*_α plots is that the Ψ versus Δ plots repeat periodically as the temperature is varied. This can be seen when comparing the $T = 73.1$°C (squares) to the 75.1°C (circles) and the $T = 73.9$°C (crosses) to the $T = 76.0$ °C (*x*'s). We believe this is due to the tight-pitch helix winding up as the temperature decreases, thereby causing the relative orientation of the top and bottom surfaces to vary in a periodic manner. The similarity of the smectic-C^*_α plots at $T = 73.1$°C (squares) and the 75.1°C (circles) to the smectic-*A* plot (down triangles) is most likely due to the two sets of surface layers being aligned in a similar manner for all three temperatures, namely, almost coplanar.

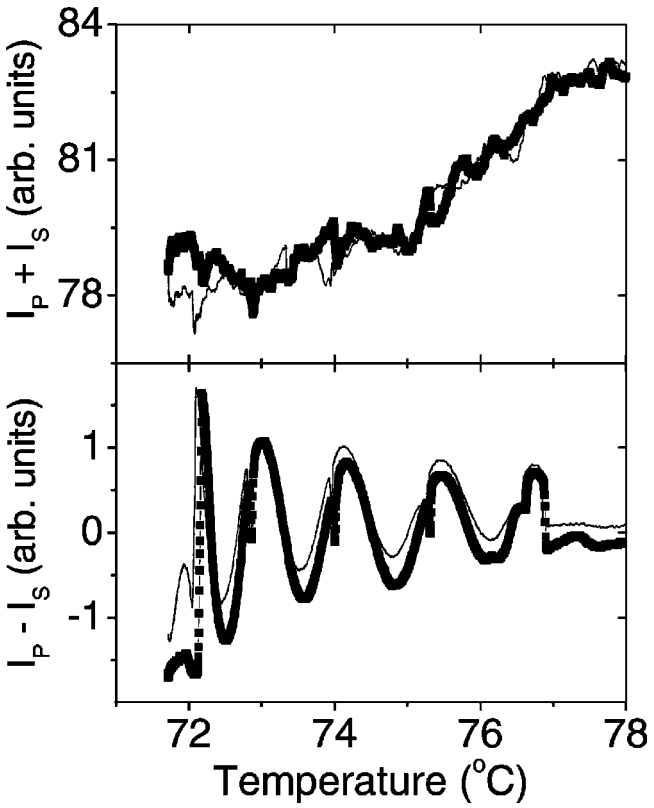

FIG. 7. Reflectivity (I_p+I_s) and (I_p-I_s) data from a 75-layer MHPBC film at different electric field orientations: $\phi_E=90°$ (large squares) and $\phi_E=270°$ (small squares).

No fits are included for the smectic-C^*_α phase because we cannot measure how the surface interfaces with the interior layers. This parameter is very important for making high, quality simulations to data taken at constant temperature. Fits will be presented below for data, taken as a function of temperature, because for this type of data, it is not as important how the surface interfaces with the interior layers as long as it does not change as a function of temperature. The constant angle between the interior and surface layers will simply cause a small offset in the pitch used to simulate the film.

Upon cooling into the smectic-C^*_{FI2} phase, the overall biaxiality of the film increased significantly, as can be seen by the width and height of the Ψ vs Δ plot. This can be seen in Fig. 6, which shows a 53-layer film at 73.1°C in the smectic-C^*_α phase (circles) and at 71.7 °C in the smectic-C^*_{FI2} phase (squares). This increase in width of the Ψ versus Δ plot is due to the change in interior layers from an optically uniaxial short-pitched helical structure in the smectic-C^*_α phase to an optically biaxial distorted structure in the smectic-C^*_{FI2} phase [9]. A simulation of the smectic-C^*_{FI2} data was made with $\theta=14.5°$, $d=35$ Å, and a distortion angle of 25°, as described by Johnson *et al.* [9].

B. High-resolution differential reflectivity

Due to an extremely tight schedule for our ellipsometry setup, and the fact that the linearly polarized reflectivity is an excellent probe for studying the smectic-C^*_α structure, we have constructed another experimental setup and significantly improved the resolution of our optical reflectivity measurements. Simple linearly polarized reflectivity can resolve the characteristic oscillations only when the reflective intensity is near the minimum, because only then is the temperature variation of the signal on the same order of magnitude as the signal itself [8]. This occurs at some film thicknesses, but not all. To remove this severe limitation and obtain high-resolution reflectivity data, we have designed and employed a differential reflectivity method [11].

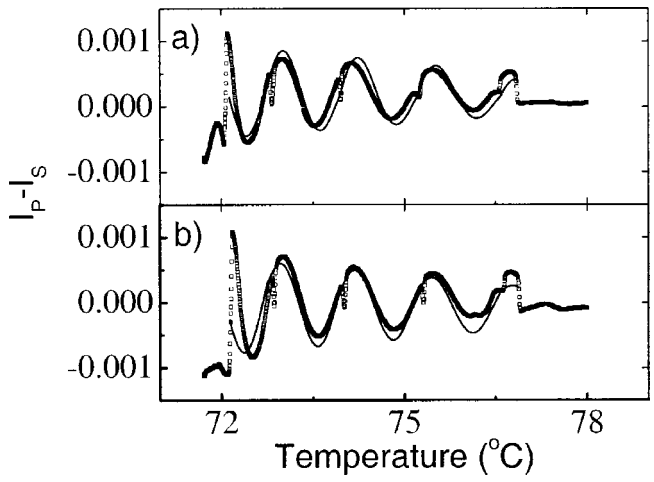

FIG. 8. Calculated reflectivity from data shown in Fig. 7 in units of the fraction of total input intensity. (a) show the data (squares) and 4×4 model results (lines) for $\phi_E=270°$, while (b) shows the data and simulations for $\phi_E=90°$. The surface structure used in modeling are three anticlinic layers per surface.

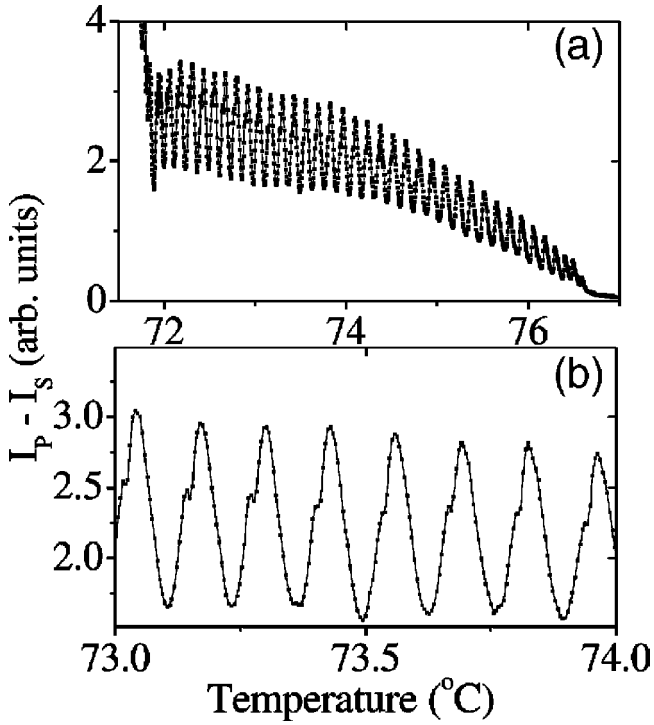

FIG. 9. Differential reflectivity data obtained from a 665-layer MHPBC film.

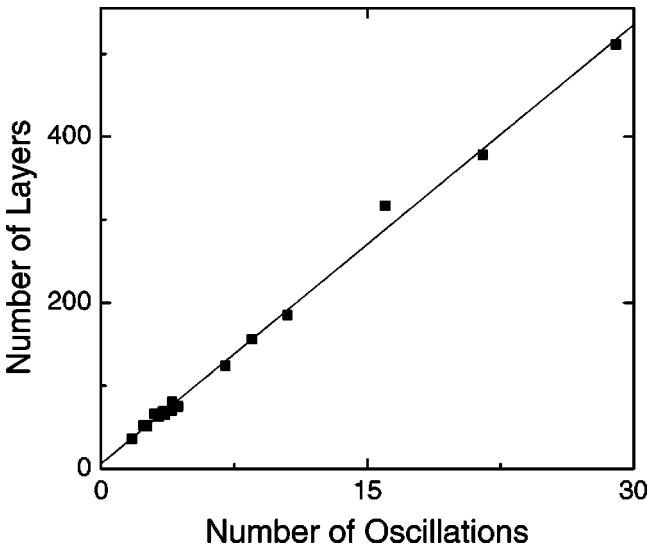

FIG. 10. Number of layers versus number of oscillations of the film in the differential (I_p-I_s) data. The vertical intercept is approximately six layers.

Our differential reflectivity system uses the following technique to measure the intensity of *s*- and *p*- polarized light reflected from a film. After passing through a Glan-Thompson polarizer and then reflecting from the free-standing film, the mechanically chopped He-Ne laser light ($\lambda = 6328$ Å) passes through a polarizing beam splitter, which separates the light into its *p*- and *s*-polarization components. Two similar photodetectors are used to monitor the intensity of each polarization component (I_p and I_s). A proper arrangement of electronics allows us to generate three output signals, namely I_p, $-I_s$ and $(I_p - I_s)$. Both $(I_p - I_s)$ and $(I_p + I_s)$ can be simultaneously acquired from two lock-in amplifiers. The differential signal $(I_p - I_s)$, is set to zero in the high-temperature range of the smectic*A* phase while the film is in its uniaxial state by rotating the incident Glan-Thompson polarizer, thereby we only measure the temperature variation of the signal. Such a differential mode operation is capable of dramatically reducing the common-mode noise before the signal is amplified.

Figure 7 shows a typical set of data, $(I_p + I_s)$ and $(I_p - I_s)$, versus temperature, from a 75-layer MHPBC film. This figure displays two sets of data acquired in cooling runs with opposite directions of applied electric field (± 2 V/cm) $\phi_E = 90°$ (large symbols) and $\phi_E = 270°$ (small ones) which are perpendicular to the incident plane of the laser beam. While the $(I_p + I_s)$ data show significant amount of noise, $(I_p - I_s)$ data is high quality. Even though we use arbitrary units for both vertical axes in Fig. 7, the ratio of the current-to-voltage conversion factors was known by using the same detectors and similar measuring schemes. Knowing the film thickness and indices of refraction enables us to get the reflectivity of the film as a fraction of the input intensity (see Fig. 8) for direct comparison with our model calculations, which will be presented below. These results indicate that the differential mode of operation allows us to improve the signal-to-noise ratio by more than several hundred.

The temperature variation of $(I_p + I_s)$ is primarily related to the change of the optical film thickness from the temperature dependence of d. The $(I_p - I_s)$ data revealed other details of the smectic-C^*_α structure. The $(I_p - I_s)$ data exhibits a discontinuous change once per oscillation. The reflectivity data for $\phi_E = 90°$ and $\phi_E = 270°$ appear to switch at the step. As discussed above, this step is due to the net polarization of the film passing through zero. Depolarized reflected light microscopy studies, near one of the steps, will be presented in Sec. II. C.

The film thickness is one of the important parameters for modeling the molecular orientational arrangements. Employ-

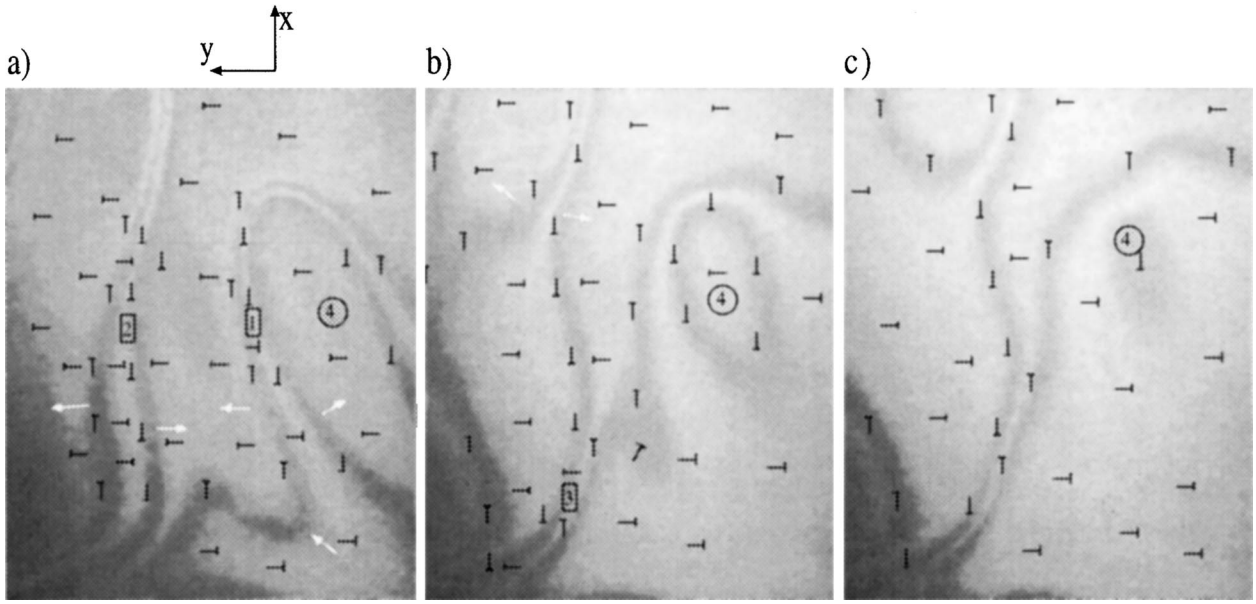

FIG. 11. Three video frames obtained during a reorientation in the smectic-C^*_α phase. The reorientation front moves from left to right. The average *c*-director orientation in each region is along the long axis of the T's. See text for detailed discussion.

ing two lasers of different wavelengths ($\lambda_1 = 0.63\ \mu$m, $\lambda_2 = 0.54\ \mu$m) and measuring the film's reflectivity as a function of the incident angle, we are able to determine the film thickness in the smectic-*A* phase [11]. The resolution is ± 2 layer for a film of several hundred smectic layers.

Differential reflectivity data from a 75- and 665-layer film, which exhibits approximately 3.5, and 37.5 oscillations in the smectic-C^*_α phase window are shown in Figs. 8 and 9, respectively. In most of the cases, the reflectivity data (see Fig. 8) are obtained from two field orientations ($\phi_E = 90°, 270°$) which are perpendicular to the incidence plane. Even for the 665-layer film, where there are 10 times as many oscillations per unit interval in temperature space as for the 75-layer film, one break in each oscillation is visible. This is shown in a smaller temperature window in Fig. 9(b). In all, films of 15 different thicknesses have been studied. Figure 10 shows *N* vs the number of oscillations. Similar to the results from 10OTBBB1M7, these data can be described by a linear relation. The finite intercept along the vertical axis suggests the existence of (6 ± 3) surface layers that do not participate with the interior layer to produce the oscillations in the data. In comparison, the 10OTBBB1M7 films have about 18 total surface layers.

To the best of our knowledge, only resonant x-ray scattering has been successfully employed to measure the pitch size (Lp$<$300 Å) of the smectic-C^*_α short-helical structure [4,6]. Because MHPBC lacks a heavy atom near its core, we have to use other means to determine the pitch. So far we have found that all the detailed experimental results from the smectic-C^* variant phases of MHPBC and 10OTBBB1M7 are qualitatively the same. Thus, similar to the 10OTBBB1M7, we will assume that the smectic-C^*_α phase has a five-layer (Lp$=5$ layers) structure just above the smectic-C^*_α - smectic-C^*_{FI2} transition. Moreover Fig. 9 displays an approximately constant oscillation frequency as a function of temperature. This strongly suggests a linear relation between the pitch and temperature. From our 665-layer film data and the aforementioned assumptions, we conclude that Lp≈ 7 near the smectic-C^*_α - smectic-*A* transition.

As discussed above, our ellipsometry measurements of many MHPBC films in the high-temperature range of the smectic*A* phase lead to $d = 35.4 \pm 0.2$ Å, $n_o = 1.482 \pm 0.002$, and $n_e = 1.64 \pm 0.01$. We have used the model depicted in Fig. 2 to simulate our data. From Fig. 10 we conclude that there are about three surface layers on each side of the film. A ξ of two layers gives the best fits. As the temperature decreases, the increase in amplitude of oscillation in $(I_p - I_s)$ indicates an increase in optical biaxiality. To account for this increase, we assume that θ_s changes from 10° to 20° throughout our fitting range. θ_b will have the power-law expression $B[(T_c - T)/T_c]^\beta$ with $\beta = 0.3$ [19] and *B* was found to be 34°. Using these parameters and employing the 4×4 matrix technique [16], we have carried out simulation of our data as shown in Fig. 8 with three anticlinic surface layers under different signs of electric-field direction. The simulation results [20] agree with our data. Thus we conclude that the model sketched in Fig. 2 gives a very good approximation of the molecular arrangements for the smectic-C^*_α phase of MHPBC as well as 10OTBBB1M7, which was studied previously [8].

C. Depolarized reflected light microscopy

Depolarized reflected light microscopy allows one to determine the orientation of the average tilt within a domain under an applied electric field. This technique uses two polarizers each at 45° to the electric field and perpendicular to each other. By decrossing the polarizers the symmetry is broken between the light polarized parallel and perpendicular to the electric field. Depending on if the polarizers are decrossed toward or away from the electric-field direction, domains that are oriented either perpendicular or parallel to the field become darker or lighter [21]. This is a powerful tool to determine the molecular orientations in the tilted liquid-crystal phases in films [22].

To gain better understanding of the break observed in each oscillation, we have used depolarized light microscopy to see the changes of the film cooling through the temperatures at which the breaks occur. Figure 11 shows three video frames that were taken during the time frame that such a break was registering in one of our reflectivity measurements. Several 2π-wall boundaries [1 and 2 in Fig. 11(a)] can be seen. Between these boundaries the orientation of the structure is in general the same, due to a weak applied electric field (2V/cm) aligning the net polarization of the film. Although the exact orientation of the different regions cannot be determined, the relative orientations can. Markers indicating the relative orientation of the structures are superimposed on the image. Light regions correspond to the structure aligned along $\pm y$, while dark regions are oriented along $\pm x$, where the x and y axis are shown on the figure. We can see that across each 2π wall the intensity has the sequence light-dark-light-dark-light. This corresponds to a rotation of the orientational structure by 2π. The free energy gained by aligning the net polarization of the majority of the film area with the applied electric field, is larger than the elastic energy cost of narrowing the 2π walls. When the field is removed, the 2π walls spread out to minimize the elastic energy cost

In the sequence (Figs. 11(a)–11(c)), the structural change moves in from the left and proceeds to the right. Initially, all regions of the film except the 2π walls are aligned in the $+y$ direction. However, as seen in Fig. 11(a), with the structural change, the middle region of the 2π wall 1, whose structure is oriented along $-y$, opens up, while the region between walls 1 and 2 begins to collapse. In Fig. 11(b), this region has been compressed so that the wall 3 is being expanded. As this process continues, we see in Fig. 11(c) that, apart from the 2π walls, the film structure is now mainly aligned in the $-y$ direction, 180° from the initial state. Also, the region that formed surrounded by a π wall (labeled 4) eventually disappears simply by rotating its structure counterclockwise. Once the process is complete, the orientational landscape of the film is completely changed, both in the alignment of the film and the location of 2π-wall defects.

These observation support the model shown in Fig. 2. The majority of the film reoriented by 180° during the change, as

should occur when the net polarization of the film passes through zero. The entire film does not change simultaneously because of a small temperature gradient across the film.

III. DISCUSSION

Similar to the 10OTBBB1M7, we have found that the smectic-C^*_α phase of MHPBC exhibits a short-pitch helical structure, which is comparable structurally to the well-known smectic-C^* phase that exhibits a pitch of optical wavelengths. However, the fact that the magnitude of pitch differs by two orders, indicates a difference in the physical origin of these helical pitches. Also, there is a heat capacity spike in the transition from smectic-C^*_α and smectic-C^*, demonstrating that the two phases are distinct [23]. The micron-sized optical helical pitch found in the smectic-C^* phase, is due to the chirality of the molecules. Unless a very strong chiral nearest-neighbor interaction can be identified, the unique nanometer-sized helical structure found in the smectic-C^*_α phase requires the competition between the interactions of the nearest-neighbor layers and those of the next-nearest-neighbor layers. Several molecular origins of the next-nearest-neighbor interaction have been proposed [24–26]. The observation of third-order x-ray diffraction peak from the molecules exhibiting the smectic-C^* variant phases [3] indicates that the smectic layer structure shows a longer correlation length than the conventional liquid-crystal compounds. Such a long positional correlation length would promote the next-nearest-neighbor interaction.

Our experimental results from the smectic-C^*_α phase of the 10OTBBB1M7 and MHPBC are similar. These results show important differences from what was found for 11HFBBB1M7 by Schlauf *et al*. The main difference may be related to their phase sequences, i.e., the occurrence or absence of low-temperature ferrielectric, ferroelectric, and antiferroelectric phases. 10OTBBB1M7 shows the ferro-, ferri-, and antiferroelectric phases, MHPBC shows the antiferro- and ferrielectric phases, and 11HFBBB1M7 shows only the ferroelectric phases. To provide more physical insight into these differences and nature of the smectic-C^*_α phase, more experimental investigations of similar compounds are essential to determine if their is a pattern to the pitch evolution in the smectic-C^*_α phase.

ACKNOWLEDGMENTS

We would like to gratefully acknowledge D. Link, B. Zeks, and M. Cepic for detailed discussions. The research was supported in part by the National Science Foundation, Solid State Chemistry Program under Grant No. DMR-9703898 and INT-9815859 and NATO International Scientific Exchange Program.

[1] A.D.L. Chandani, E. Gorecka, Y. Ouchi, H. Takezoe, and A. Fukuda, Jpn. J. Appl. Phys., Part 2 **28**, L1265 (1989).
[2] A. Fukuda, Y. Takanishi, T. Isozaki, K. Ishikawa, and H. Takezoe, J. Mater. Chem. **4**, 997 (1994). This review includes a summary of smectic-C^* variant phases.
[3] Y. Takanishi, A. Ikeda, H. Takezoe, and A. Fukuda, Phys. Rev. E **51**, 400 (1995).
[4] P. Mach, R. Pindak, A.-M. Levelut, P. Barois, H.T. Nguyen, C.C. Huang, and L. Furenlid, Phys. Rev. Lett. **81**, 1015 (1998).
[5] T. Matsumoto, A. Fukuda, M. Johno, Y. Motoyama, T. Yui, S. Seomun, and M. Yamashita, J. Mater. Chem. **9**, 2051 (1999).
[6] P. Mach, R. Pindak, A.-M. Levelut, P. Barois, H.T. Nguyen, H. Baltes, M. Hird, K. Toyne, A. Seed, J.W. Goodby, C.C. Huang, and L. Furenlid, Phys. Rev. E **60**, 6793 (1999).
[7] L.S. Matkin, H.F. Gleeson, P. Mach, C.C. Huang, R. Pindak, G. Srajer, J. Pollmann, J.W. Goodby, M. Hird, and A. Seed, Appl. Phys. Lett. **76**, 1863 (2000).
[8] P.M. Johnson, S. Pankratz, P. Mach, H.T. Nguyen, and C.C. Huang, Phys. Rev. Lett. **83**, 4073 (1999).
[9] P.M. Johnson, D.A. Olson, S. Pankratz, T. Nguyen, J. Goodby, M. Hird, and C.C. Huang, Phys. Rev. Lett. **84**, 4870 (2000).
[10] D. Schlauf, Ch. Bahr, and H.T. Nguyen, Phys. Rev. E **60**, 6816 (1999).
[11] S. Pankratz, P.M. Johnson, and C.C. Huang, Rev. Sci. Instrum. **71**, 3184 (2000).
[12] D.A. Olson, A. Cady, P.M. Johnson, X.F. Han, and C.C. Huang (unpublished).
[13] P.M. Johnson, D.A. Olson, S. Pankratz, Ch. Bahr, J.W. Goodby, and C.C. Huang, Phys. Rev. E **62**, 8106 (2000).
[14] R. Geer, T. Stoebe, and C.C. Huang, Phys. Rev. E **48**, 408 (1993).
[15] The temperatures were measured by thermisters near the film plate. The small temperature offset between the film and the thermocouples is not equal in both systems.
[16] D.W. Berreman, J. Opt. Soc. Am. **62**, 502 (1972).
[17] R.M.A. Azzam and N. M. Bashara, *Ellipsometry and Polarized Light* (North-Holland, Amsterdam, 1989).
[18] A minor error was found in our previous determination of Δ. The correct values of Δ are offset by 180° from what was previously reported, but this does not affect the values of other reported physical quantities.
[19] C.C. Huang and J.M. Viner, Phys. Rev. A **25**, 3385 (1982); C. C. Huang and J. M. Viner, in *Liquid Crystals and Ordered Fluids*, edited by A. C. Griffin and J. F. Johnson (Plenum New York, 1984), Vol. 4, p. 643.
[20] We have tried two other surface-layer arrangements: three synclinic layers and two anticlinic layer. The results for these configurations are not as good as the one reported here.
[21] R. Pindak, C.Y. Young, R.B. Meyer, and N.A. Clark, Phys. Rev. Lett. **45**, 1193 (1980).
[22] D.R. Link, G. Natale, R. Shao, J.E. Maclennan, N.A. Clark, E. Korblova, and D.M. Walba, Science **278**, 1924 (1997).
[23] K. Ema, H. Yao, I. Kawamura, T. Chan, and C.W. Garland, Phys. Rev. E **47**, 1203 (1993).
[24] K. Yamada, Y. Takanishi, K. Ishikawa, H. Takezoe, A. Fukuda, and M.A. Osipov, Phys. Rev. E **56**, R43 (1997).
[25] R. Bruinsma and J. Prost, J. Phys. II **4**, 1209 (1994).
[26] B. Rovšek, M. Čepič, and B. Žekš, Phys. Rev. E **62**, 3758 (2000).